Rapid Communications

Controlled transport between Fermi superfluids through a quantum point contact

Juan Yao,[1] Boyang Liu,[2,*] Mingyuan Sun,[1] and Hui Zhai[1,3]
[1]*Institute for Advanced Study, Tsinghua University, Beijing 100084, China*
[2]*Institute of Theoretical Physics, Beijing University of Technology, Beijing 100124, China*
[3]*Collaborative Innovation Center of Quantum Matter, Beijing 100084, China*

(Received 1 January 2018; published 8 October 2018)

Recent advances in experimental techniques allow one to create a quantum point contact between two Fermi superfluids in cold atomic gases with a tunable transmission coefficient. In this Rapid Communication we propose that three distinct behaviors of charge transports between two Fermi superfluids can be realized in this single setup, which are the multiple Andreev reflection, the self-trapping, and the Josephson oscillation. We investigate the dynamics of atom number difference between two reservoirs for different initial conditions and different transmission coefficients, and present a coherent picture of how the crossover between different regimes takes place. Our results can now be directly verified in the current experimental system.

DOI: 10.1103/PhysRevA.98.041601

Introduction. Transport measurements are powerful tools not only for revealing fundamental properties of quantum materials in condensed-matter physics, but also for constructing solid-state devices. In the past few years, transport has also become one of the frontiers in cold atom physics. Various experiments have been conducted, including particle transport [1–7], heat transport [8], and spin transport [9–13]. Of particular interest is the realization of the two-terminal transport measurements in a cold atom setup [1–6,8]. As shown in Fig. 1(a), a cigar-shaped cloud is split into two reservoirs and connected by a quantum point contact (QPC) generated by high-resolution lithography [2,4,5]. With this setup, in the weakly interacting regime, quantized conductance of neutral matter has been first observed [2]. In the strongly interacting regime, both multiple Andreev reflections between two Fermi superfluids and anomalous transport between two normal gases have been observed [4,5], the latter of which has attracted considerable attention for the lack of theoretical consensus on its origin [14–17].

One great advantage of studying transport with cold atoms is to utilize the tunability of this system to cover different physics in different parameter regimes in a single setting, and therefore to reveal how the transition between them takes place. Here we focus on the case of the Fermi superfluid. One well-known transport effect is the Josephson effect, which is a nondissipative coherent oscillation. It was first predicted and observed in condensed-matter systems [18,19] and then has been intensively studied in superconductors [20]. In cold atom experiments this effect has also been observed for both Bose and Fermi superfluids [3,21] and theoretical investigations have also been conducted [22–27]. Besides the nondissipative Josephson effect, the dissipative transport can also take place in fermionic superfluids [7,28]. In the experiment of Ref. [4], when two Fermi superfluids are connected by a QPC, the time evolution of the particle number difference between two reservoirs exhibits a nonexponential decay, which can be well explained by the multiple Andreev reflections [29].

Then, a question is raised naturally. For transport between two Fermi superfluids, under what condition does it exhibit the Josephson effect and under what condition does it exhibit the multiple Andreev reflections? In fact, the single-particle transmission coefficient plays a crucial role in answering this question. A small transmission coefficient favors the Josephson effect and a large transmission coefficient favors the multiple Andreev reflections. Fortunately, recently a new technique allows one to continuously tune the transmission coefficient in the cold atom QPC setup by imprinting a mesoscopic potential or a lattice into the tunneling channel with a digital micromirror device (DMD) [6,30]. The key point of this Rapid Communication is to propose that one can use this new technology to tune the transport between two Fermi superfluids, with which one can observe and understand the crossover from the multiple Andreev reflection type transport to the self-trapping and the Josephson type transport. This will provide a unified view of these seemingly disparate transport phenomena.

Setup. The setup of a QPC for a cold atom system is schematically shown in Fig. 1(a). First of all, two beams provide transverse harmonic confinements along the $\hat{x}$ and $\hat{z}$ directions, respectively, whose confinement frequencies vary smoothly along the longitudinal transport direction $\hat{y}$. That is to say, in a first quantized form, the Hamiltonian for the QPC regime can be written as

$$\hat{H} = \frac{\mathbf{p}^2}{2m} + \frac{1}{2m}\omega_x^2(y)x^2 + \frac{1}{2m}\omega_z^2(y)z^2 + V_{\mathrm{DMD}}(y), \quad (1)$$

where $\omega_i(y) = \omega_i^0 e^{-y^2/d_i^2}$ $(i = x, z)$. Here typical values for experiment are $\hbar\omega_x^0 \sim 12E_F$, $\hbar\omega_z^0 \sim 4E_F$, $d_x \sim 3.6/k_F$, and $d_z \sim 18.2/k_F$ with total number of particles $N \sim 2 \times 10^5$. Because $d_z > d_x$, it first squeezes the system into a quasi-two-dimensional plane and then to a quasi-one-dimensional tunnel. Secondly, another beam provides a gate potential

*byliu@bjut.edu.cn

 ©2018 American Physical Society

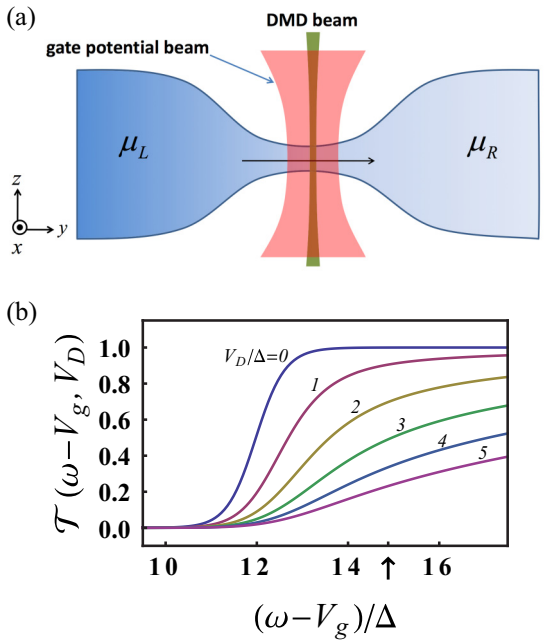

FIG. 1. (a) The geometry of the experimental setup. Two reservoirs are connected by a QPC. A gate beam applied on the central regime tunes the relative energy V_g between the QPC and the reservoirs. A tightly focused DMD beam tunes the tunneling amplitude. (b) The transmission coefficient $\mathcal{T}$ as a function of ω is plotted for different V_D. For later convenience, we have taken the bulk pairing gap Δ as the energy unit and we choose $\hbar\omega_x^0/\Delta = 18$ and $\hbar\omega_z^0/\Delta = 6$.

that generates a uniform energy shift V_g between the regime of QPC and the reservoir. That is to say, when we consider an incoming state whose asymptotic behavior is a plane wave with momentum k_y, the energy conservation gives $\omega - V_g = \hbar^2 k_y^2/(2m)$ with the particle energy being ω. Finally, a DMD beam can generate one or a sequence of delta-function potentials inside the quasi-one-dimensional tunneling channel. For the simplest case, we first consider $V_{\rm DMD}(y) = V_{\rm D}\delta(y)$.

In practice, V_g and $V_{\rm D}$ are two parameters that can be easily tuned. By solving this QPC Hamiltonian, one can obtain the transmission coefficient $\mathcal{T}$, as shown in Fig. 1(b). Without $V_{\rm DMD}(y)$, the potential varies sufficiently smoothly in space such that $\mathcal{T}$ sharply jumps from zero to unity, when the incoming energy E increases beyond the threshold $\hbar(\omega_x^0 + \omega_z^0)/2$ and one of the tunneling channels becomes open, as shown by the $V_{\rm D} = 0$ curve in Fig. 1(b). For finite $V_{\rm D}$, $\mathcal{T}$ varies much more smoothly as ω varies. Consequently, for a fixed energy ω above the threshold, $\mathcal{T}$ continuously decreases as $V_{\rm D}$ increases. In this way, we can tune the transmission coefficient in this system. In Fig. 1(b) we use an arrow to label the position of $\mu_R - V_g$, the value of which we will use in the later calculation, and the transmission coefficient $\mathcal{T}$ decreases continuously as $V_{\rm D}$ increases for the incoming particle with energy equaling to the chemical potential μ_R.

Model and method. Firstly, we take a mean-field Hamiltonian to describe the Fermi superfluids in the left and the right reservoirs, which reads

$$\hat{H}_j = \sum_{\mathbf{k}\sigma} \xi_{j\mathbf{k}} \hat{\psi}^\dagger_{j\sigma}(\mathbf{k})\hat{\psi}_{j\sigma}(\mathbf{k}) - \Delta_j \hat{\psi}_{j\uparrow}(\mathbf{k})\hat{\psi}_{j\downarrow}(-\mathbf{k}) + \text{H.c.}, \tag{2}$$

where $j = L, R$ is the reservoir index, $\sigma = \uparrow, \downarrow$ labels spin index, and $\xi_{j\mathbf{k}} = \mathbf{k}^2/(2m) - \mu_j$. The parameters μ_j and Δ_j are the chemical potential and the order parameter of the j-th reservoir, respectively. Here, as an example, we will take $\mu/E_{\rm F} = 0.59$ and $\Delta/E_{\rm F} = 0.68$ as typical values for unitary Fermi gas.

Secondly, to study the transport behavior, we employ the nonequilibrium Keldysh formalism, for which we introduce the forward and backward branches of the time contours and denote them by $\alpha = 1, 2$ after the Keldysh rotation [31]. Since later we will model the QPC as a local tunneling from the left to the right reservoirs, we introduce

$$\hat{\psi}_{j\alpha\sigma}(\omega - \mu_j) = \int dt\, \hat{\psi}_{j\alpha\sigma}(\mathbf{r} = 0, t) e^{i(\omega - \mu_j)t}, \tag{3}$$

where ω is defined as the absolute energy of the particles, and thus $\omega - \mu_j$ is the energy measured with respect to the chemical potential of the jth reservoir. Here we define a spinor as $\hat{\Psi}(\omega) = [\hat{\Psi}_L(\omega - \mu_L), \hat{\Psi}_R(\omega - \mu_R)]^T$ with

$$\hat{\Psi}_j(\omega - \mu_j) = \begin{bmatrix} \hat{\psi}_{j1\uparrow}(\omega - \mu_j) \\ \hat{\psi}^\dagger_{j2\downarrow}(\overline{\omega - \mu_j}) \\ \hat{\psi}_{j2\uparrow}(\omega - \mu_j) \\ \hat{\psi}^\dagger_{j1\downarrow}(\overline{\omega - \mu_j}) \end{bmatrix}, \tag{4}$$

where $\overline{\omega - \mu_j} = -(\omega - \mu_j)$ and "T" denotes the transposition. The bare Green's function $\mathcal{G}_0 = \langle \hat{\Psi}(\omega)\hat{\Psi}^\dagger(\omega)\rangle$ is therefore an 8×8 matrix for a given ω. The left and right reservoirs are decoupled without tunneling, then $\mathcal{G}_0(\omega)$ is

$$\mathcal{G}_0(\omega) = \begin{pmatrix} \mathcal{G}_{0L}(\omega) & 0 \\ 0 & \mathcal{G}_{0R}(\omega) \end{pmatrix}. \tag{5}$$

Each $\mathcal{G}_{0j=L,R}$ is a 4×4 matrix of the form [32–34]

$$\mathcal{G}_{0j}(\omega) = \begin{bmatrix} \mathcal{G}_j^R(\omega) & \mathcal{G}_j^K(\omega) \\ 0 & \mathcal{G}_j^A(\omega) \end{bmatrix}, \tag{6}$$

where $\mathcal{G}_j^R(\omega)$, $\mathcal{G}_j^A(\omega)$, and $\mathcal{G}_j^K(\omega)$ are the retarded, advanced, and Keldysh Green's functions, respectively. Considering that each reservoir is in the thermal equilibrium, the Keldysh component of the Green's function can be obtained as $\mathcal{G}_j^K(\omega) = \tanh(\frac{\omega - \mu_j}{2T})[\mathcal{G}_j^R(\omega) - \mathcal{G}_j^A(\omega)]$ at temperature T. The mean-field Hamiltonian gives the retarded and the advanced Green's functions as [32–34]

$$\mathcal{G}^{R(A)}(\omega) = \frac{1}{\sqrt{\Delta_j^2 - (\omega - \mu_j \pm i0^+)^2}} \times \begin{bmatrix} -(\omega - \mu_j \pm i0^+) & \Delta_j \\ \Delta_j & -(\omega - \mu_j \pm i0^+) \end{bmatrix}. \tag{7}$$

It is straightforward to calculate the inverse of the bare Green's function as

$$\mathcal{G}_{0j}^{-1} = \begin{bmatrix} (\mathcal{G}_j^R)^{-1} & (\mathcal{G}_j^{-1})^K \\ 0 & (\mathcal{G}_j^A)^{-1} \end{bmatrix}, \tag{8}$$

where $(\mathcal{G}_j^{-1})^K = -(\mathcal{G}_j^R)^{-1}\mathcal{G}_j^K(\mathcal{G}_j^A)^{-1}$.

Thirdly, the tunneling between two reservoirs is modeled by local tunnelings as [32–34]

$$\mathcal{V} = \int_{-\infty}^{\infty} \frac{d\omega}{2\pi} \sum_{\sigma,\alpha=1,2} \{\mathcal{T}(\omega - V_g, V_D) \times \hat{\psi}^\dagger_{L\alpha\sigma}(\omega - \mu_L)\hat{\psi}_{R\alpha\sigma}(\omega - \mu_R) + \text{H.c.}\}, \tag{9}$$

where the transmission amplitude $\mathcal{T}(\omega - V_g, V_D)$ is a function of V_g and V_D as discussed above. Thus, the inverse of the full Green's function $\mathcal{G}^{-1}$ can be calculated by incorporating $\mathcal{G}_0^{-1}$ with a matrix form of $\mathcal{V}$. Since $\mathcal{V}$ introduces coupling between different frequencies, $\mathcal{G}^{-1}$ will not be a simple 8×8 matrix as $\mathcal{G}_0^{-1}$. Hence, in practice, we discretize the frequency space and write down an infinite matrix of $\mathcal{G}^{-1}$, and then numerically calculate the inverse of it [35].

Finally, it is convenient to calculate the current $I(t) = \frac{1}{2}\partial(N_R - N_L)/\partial t$ in the frequency space by introducing

$$I(t) = \int_{-\infty}^{\infty} \frac{d\Omega}{2\pi} I(\Omega) e^{-i\Omega t}, \tag{10}$$

and in the Keldysh formalism the current $I(\Omega)$ is written as

$$\begin{aligned} I(\Omega) = -\frac{i}{2}\sum_\sigma \int_{-\infty}^{\infty} \frac{d\omega}{2\pi} \{&\mathcal{T}(\omega - V_g, V_D) \\ &\times \langle \hat{\psi}_{R1\sigma}(\omega - \mu_R + \Omega)\hat{\psi}^\dagger_{L2\sigma}(\omega - \mu_L)\rangle \\ &- \mathcal{T}(\omega - V_g, V_D)\langle \hat{\psi}_{L1\sigma}(\omega - \mu_L + \Omega) \\ &\times \hat{\psi}^\dagger_{R2\sigma}(\omega - \mu_R)\rangle\}. \end{aligned}$$

With the Green's function calculated above, it is straightforward to obtain $I(\Omega)$. Here the frequency Ω can only take a series of discrete values as $\Omega_m = 2m\delta\mu$ with $m = 0, \pm1, \pm2, \ldots$ [32], where $\delta\mu = \mu_L - \mu_R$ is the bias voltage. Denoting $I(\Omega_m) \equiv I_m$, the total current for a fixed bias voltage can be written as

$$I(t) = I_0 + 2\sum_{m=1}^{\infty} [\text{Re}(I_m)\cos(\Omega_m t) + \text{Im}(I_m)\sin(\Omega_m t)]. \tag{11}$$

Controlled transport. In Fig. 2, we first show the current I_0 and I_1 as functions of V_D/Δ and $\delta\mu/\Delta$. We have verified that the higher component currents are much smaller than these two and can be safely ignored. The I_0 part is the dc component, which results from the quasiparticle transport by the multiple Andreev reflections. The components of $\text{Re}(I_1)\cos(\Omega_1 t)$ and $\text{Im}(I_1)\sin(\Omega_1 t)$ are the ac parts and are usually referred to as the "cosine" and "sine" terms. They describe the phase coherent transport of the Cooper pairs [20]. The sine term $\text{Im}(I_1)\sin(\Omega_1 t)$ is related to the usual Josephson current. The cosine term was also predicted by Josephson [18] originally. It was first observed in the experiment by Pederson *et al.* [36]. In the usual weak link discussion, the cosine term vanishes in the first order of perturbation theory, and presents at the second-order calculation.

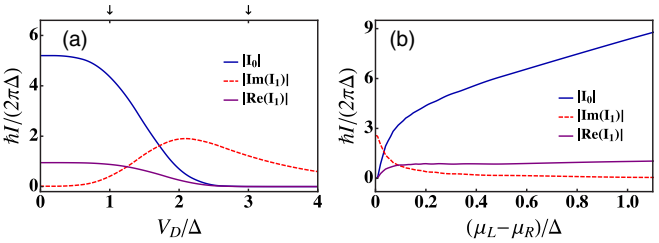

FIG. 2. $|I_0|$, and the real and imaginary parts of I_1 as a function of V_D/Δ for fixed $\delta\mu = 0.2\Delta$ (a), and as a function of $\delta\mu/\Delta$ for fixed $V_D = \Delta$ (b). Here we have fixed $V_g = -14\Delta$.

Because the dc current is generated by the multiple Andreev reflection, if n is the smallest integer such that $n\delta\mu > 2\Delta$, it takes at least $(2n-1)$ step of tunnelings in order to generate the dc current, and therefore the current is proportional to $\mathcal{T}^{2n}$ [32,34]. Thus, the dc current is dominative either when V_D is small and $\mathcal{T}$ is close to unity, as shown in Fig. 2(a), or when $\delta\mu$ is larger compared to Δ and n is small, as shown in Fig. 2(b). In other words, when either V_D increases and $\mathcal{T}$ decreases, or when $\delta\mu$ becomes small, the dc current gradually decreases until vanishing. In these two regimes, the Josephson current will become dominative, as one can also see from Fig. 2.

In realistic cold atom experiments, instead of studying transport with a fixed bias voltage as in a condensed-matter system, one starts with an initial atom number imbalance and monitors how this imbalance evolves as a function of time. To investigate this dynamics, we employ coupled dynamical equations as follows:

$$\begin{aligned} \frac{d\delta n}{dt} &= -I_0 - 2\text{Re}(I_1)\cos\phi - 2\text{Im}(I_1)\sin\phi, \\ \frac{d\phi}{dt} &= 2\delta\mu(t), \end{aligned} \tag{12}$$

where ϕ is the phase difference between the two reservoirs, and $\delta\mu$ is related to the atom imbalance by

$$\frac{\mu_L}{\mu_R} = \left(\frac{1+\delta n}{1-\delta n}\right)^{2/3} \tag{13}$$

and $\delta n = (N_L - N_R)/(N_L + N_R)$. Here the major assumption is that the tunneling time is much longer than the local equilibrium time of the reservoir (characterized by $t_F = 2\pi\hbar/E_F$), such that we can apply the above results with fixed $\delta\mu$ to any instantaneous time. From the results we obtained (as shown in Fig. 3), this assumption is indeed well obeyed.

The different regimes of tunneling dynamics are summarized in Fig. 3 with two tunable parameters δn and V_D. Let us analyze the evolution between different regimes as follows.

A → B: In case A, I_0 is the most dominative component and δn quickly drops to zero. From case A to case B, the initial δn decreases. Because I_0 is less dominative in the small $\delta\mu$ regime, as shown in Fig. 3(b), one can see that a small oscillation of δn becomes visible, and at mean time the

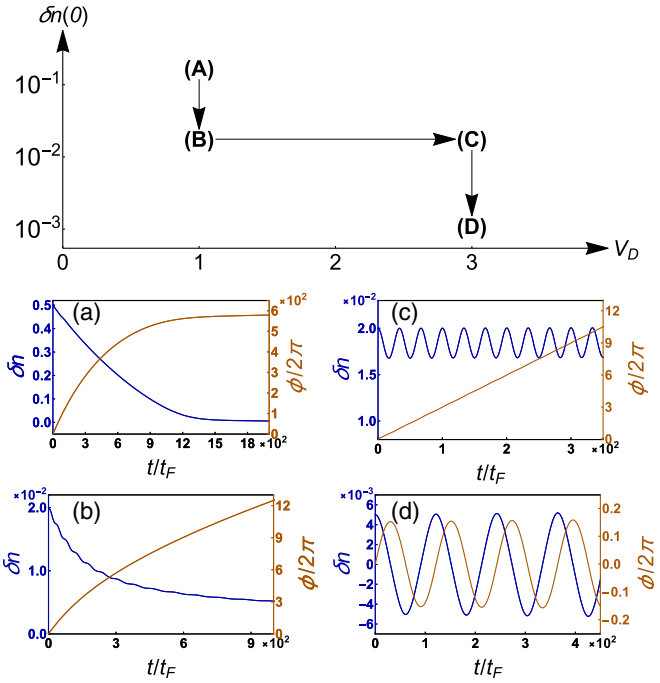

FIG. 3. Schematic of different transport regimes with different initial atom number difference δn and different V_D. (a)–(d) represent four typical dynamical behaviors for δn and ϕ. For (a), $\delta n(0) = 0.5$, $V_D = \Delta$, and corresponding $\mathcal{T} \sim 0.9$. (b) has the same V_D and $\mathcal{T}$ as (a), but smaller initial $\delta n(0) = 0.02$. For (c), $\delta n(0) = 0.02$, $V_D = 3\Delta$, and corresponding $\mathcal{T} \sim 0.5$. (d) has the same V_D and $\mathcal{T}$ as (c), but different initial $\delta n(0) = 0.005$.

long-time saturation value of δn is a finite value instead of dropping to zero.

B → C: From case B to case C, the initial δn is about the same, but V_D increases and $\mathcal{T}$ decreases. The Josephson effect gradually becomes dominant over the multiple Andreev reflection. This crossover happens in the way that on one hand, the saturation value of δn increases until eventually the drop of δn becomes insignificant, and on the other hand, the oscillation becomes more profound. As a result, δn oscillates around a finite value. This is known as the "self-trapping" regime in the previous study of the Josephson oscillations in a Bose-Einstein condensate of bosons [22].

C → D: In both cases of C and D, V_D and $\mathcal{T}$ are fixed in the regime where $\mathrm{Im}(I_1)$ is the most dominative component. The only difference is that the initial δn in case D is much smaller than that of case C. Only keeping the $\sin\phi$ term in the first equation of Eq. (12), it is known that Eq. (12) can be mapped to the dynamical equation of a classical pendulum, where two different solutions can be found depending on the initial conditions. The first is an oscillation around the global minimum when δn is small, corresponding to the conventional Josephson effect, and the other is a continuous clockwise (or anticlockwise) rotation when δn is large, corresponding to the

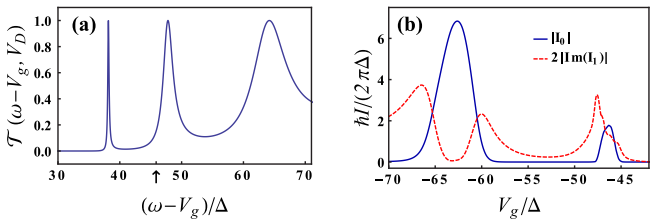

FIG. 4. (a) The transmission amplitude $\mathcal{T}(\omega - V_g, V_D)$ for the case of two delta-function potentials with $V_D = 8\Delta$. (b) The currents I_0 and $\mathrm{Im}(I_1)$ as functions of the gate potential for a fixed chemical potential bias $\delta\mu = 0.6\Delta$.

self-trapping [22]. A similar crossover from the Josephson to the self-trapping regime has also been observed previously in a Bose condensate of bosons [21].

Tuning transport with gate potential. For a single delta-function potential barrier, $\mathcal{T}$ is a monotonic function of $\omega - V_g$ as shown in Fig. 1(b). For multiple delta-function potentials, due to the interference effect, $\mathcal{T}$ as a function of $\omega - V_g$ exhibits much richer structure, as shown in Fig. 4(a). When the gate potential is applied to the QPC region, the energy of the eigenmode in QPC is lowered by V_g. This is equivalent to shifting the chemical potentials of the reservoirs. In Fig. 4(a) we label the position of the chemical potential of the right reservoir by an arrow. Hence as one increases $|V_g|$, the arrow moves from left to right. The particles around the chemical potential will see a varying $\mathcal{T}$. As we discussed in Fig. 2, when one varies $\mathcal{T}$ the relative strength between I_0 and $\mathrm{Im}(I_1)$ will change. Eventually, the varying V_g can lead to an oscillating behavior of I_0 and $\mathrm{Im}(I_1)$ as shown in Fig. 4(b). Thus, in this case, the different regimes of transport behaviors discussed above can also be controlled by V_g instead of V_D.

Outlook. In summary, we have presented a system in which three distinct behaviors of transport between two Fermi superfluids can all be realized, and the crossover between them can be tuned by both the initial atom number imbalance and the transmission coefficient. Given that the experimental technique required has been reported, our prediction can now be directly applied to current experimental setup. Further investigation along this direction includes the multichannel effect and finite temperature effect. The similar argument as presented above will lead to the conclusion that the multichannel effect may suppress the Josephson effect. Finite temperature effect can affect the stabilization of the self-trapping because of the suppression of the order parameter and the increasing of the quasiparticle excitations. Generalization of this study can also be extended to spin and heat transport problems with a tunable transmission coefficient through a quantum point contact.

Acknowledgments. The numerical calculation was done at National Supercomputer Centre in Guangzhou. We would like to thank Shizhong Zhang and Shun Uchino for discussions. This work is supported by MOST under Grant No. 2016YFA0301600 and NSFC Grant No. 11734010.

[1] D. Stadler, S. Krinner, J. Meineke, J.-P. Brantut, and T. Esslinger, Nature (London) **491**, 736 (2012).

[2] S. Krinner, D. Stadler, D. Husmann, J.-P. Brantut, and T. Esslinger, Nature (London) **517**, 64 (2015).

[3] G. Valtolina, A. Burchianti, A. Amico, E. Neri, K. Xhani, J. A. Seman, A. Trombettoni, A. Smerzi, M. Zaccanti, M. Inguscio, and G. Roati, Science **350**, 1505 (2015).
[4] D. Husmann, S. Uchino, S. Krinner, M. Lebrat, T. Giamarchi, T. Esslinger, and J.-P. Brantut, Science **350**, 1498 (2015).
[5] S. Krinner, M. Lebrat, D. Husmann, C. Grenier, J.-P. Brantut, and T. Esslinger, Proc. Natl. Acad. Sci. U.S.A. **113**, 8144 (2016).
[6] S. Häusler, S. Nakajima, M. Lebrat, D. Husmann, S. Krinner, T. Esslinger, and J.-P. Brantut, Phys. Rev. Lett. **119**, 030403 (2017).
[7] A. Burchianti, F. Scazza, A. Amico, G. Valtolina, J. A. Seman, C. Fort, M. Zaccanti, M. Inguscio, and G. Roati, Phys. Rev. Lett. **120**, 025302 (2018).
[8] J.-P. Brantut, C. Grenier, J. Meineke, D. Stadler, S. Krinner, C. Kollath, T. Esslinger, and A. Georges, Science **342**, 713 (2013).
[9] A. Sommer, M. Ku, G. Roati, and M. W. Zwierlein, Nature (London) **472**, 201 (2011).
[10] A. B. Bardon, S. Beattie, C. Luciuk, W. Cairncross, D. Fine, N. S. Cheng, G. J. A. Edge, E. Taylor, S. Zhang, S. Trotzky, and J. H. Thywissen, Science **344**, 722 (2014).
[11] M. Koschorreck, D. Pertot, E. Vogt, and M. Kohl, Nat. Phys. **9**, 405 (2013).
[12] C. Luciuk, S. Smale, F. Bottcher, H. Sharum, B. A. Olsen, S. Trotzky, T. Enss, and J. H. Thywissen, Phys. Rev. Lett. **118**, 130405 (2017).
[13] G. Valtolina, F. Scazza, A. Amico, A. Burchianti, A. Recati, T. Enss, M. Inguscio, M. Zaccanti, and G. Roati, Nat. Phys. **13**, 704 (2017).
[14] B. Liu, H. Zhai, and S. Zhang, Phys. Rev. A **90**, 051602(R) (2014).
[15] M. Kanász-Nagy, L. Glazman, T. Esslinger, and E. A. Demler, Phys. Rev. Lett. **117**, 255302 (2016).
[16] B. Liu, H. Zhai, and S. Zhang, Phys. Rev. A **95**, 013623 (2017).
[17] S. Uchino and M. Ueda, Phys. Rev. Lett. **118**, 105303 (2017).
[18] B. D. Josephson, Phys. Lett. **1**, 251 (1962).
[19] P. W. Anderson and J. M. Rowell, Phys. Rev. Lett. **10**, 230 (1963).
[20] A. Barone and G. Paterno, *Physics and Applications of the Josephson Effect* (Wiley, New York, 1982).
[21] M. Albiez, R. Gati, J. Fölling, S. Hunsmann, M. Cristiani, and M. K. Oberthaler, Phys. Rev. Lett. **95**, 010402 (2005).
[22] A. Smerzi, S. Fantoni, S. Giovanazzi, and S. R. Shenoy, Phys. Rev. Lett. **79**, 4950 (1997).
[23] I. Zapata, F. Sols, and A. J. Leggett, Phys. Rev. A **57**, R28 (1998).
[24] P. Villain and M. Lewenstein, Phys. Rev. A **59**, 2250 (1999).
[25] A. Vardi and J. R. Anglin, Phys. Rev. Lett. **86**, 568 (2001).
[26] M. Holthaus and S. Stenholm, Eur. Phys. J. B **20**, 451 (2001).
[27] F. Meier and W. Zwerger, Phys. Rev. A **64**, 033610 (2001).
[28] M. Delehaye, S. Laurent, I. Ferrier-Barbut, S. Jin, F. Chevy, and C. Salomon, Phys. Rev. Lett. **115**, 265303 (2018).
[29] A. F. Andreev, Sov. Phys. JETP **19**, 1228 (1964).
[30] M. Lebrat, P. Grišins, D. Husmann, S. Häusler, L. Corman, T. Giamarchi, J.-P. Brantut, and T. Esslinger, Phys. Rev. X **8**, 011053 (2018).
[31] A. Kamenev, *Field Theory of Non-Equilibrium Systems* (Cambridge University Press, Cambridge, UK, 2011).
[32] J. C. Cuevas, A. Martín-Rodero, and A. Levy Yeyati, Phys. Rev. B **54**, 7366 (1996).
[33] C. J. Bolech and T. Giamarchi, Phys. Rev. Lett. **92**, 127001 (2004).
[34] C. J. Bolech and T. Giamarchi, Phys. Rev. B **71**, 024517 (2005).
[35] See Supplemental Material at http://link.aps.org/supplemental/10.1103/PhysRevA.98.041601 for a detailed discussion of calculating the full Green's function.
[36] N. F. Pederson, T. F. Finnegan, and D. N. Langenberg, Phys. Rev. B **6**, 4151 (1972).